Available online at www.sciencedirect.com
ScienceDirect
Icarus 196 (2008) 202–215
ICARUS
www.elsevier.com/locate/icarus

The coating hypothesis for ammonia ice particles in Jupiter: Laboratory experiments and optical modeling

Konstantinos S. Kalogerakis [a,*], Jochen Marschall [a], Anand U. Oza [a,1], Patricia A. Engel [a,2], Rhiannon T. Meharchand [a,3], Michael H. Wong [b]

[a] *Molecular Physics Laboratory, SRI International, Menlo Park, CA 94025, USA*
[b] *Astronomy Department, University of California, Berkeley, CA 94720-3411, USA*

Received 19 December 2007; revised 1 March 2008

Available online 19 March 2008

Abstract

We report laboratory experiments and modeling calculations investigating the effect of a hydrocarbon coating on ammonia ice spectral signatures. Observational evidence and thermochemical models indicate an abundance of ammonia ice clouds in Jupiter's atmosphere. However, spectrally identifiable ammonia ice clouds are found covering less than 1% of Jupiter's atmosphere, notably in areas of strong vertical transport, indicating a short lifetime for the signature of ammonia absorption on condensed ammonia particles [Baines, K.H., Carlson, R.W., Kamp, L.W., 2002. Icarus 159, 74–94]. Current literature has suggested coating of ammonia ice particles by a hydrocarbon haze as a possible explanation for this paradox. The work presented here supports the inference of a coating effect that can alter or suppress ammonia absorption features. In the experiments, thin films of ammonia ices are deposited in a cryogenic apparatus, coated with hydrocarbons, and characterized by reflection-absorption infrared spectroscopy. We have observed the effects on the ammonia ice absorption features near 3 and 9 μm with coverage by thin layers of hydrocarbons. Modeling calculations of these multilayer thin films assist in the interpretation of the experimental results and reveal the important role of optical interference in altering the aforementioned ammonia spectral features. Mie and T-matrix scattering calculations demonstrate analogous effects for ammonia ice particles and investigate the relative effects of ammonia ice particle size, shape, and coating layer thickness on the ice particle spectral signatures.

Keywords: Jupiter, atmosphere; Ices, IR spectroscopy; Jovian planets

1. Introduction

One-dimensional chemical thermodynamic equilibrium models for Jupiter predict three cloud layers, whose bases depend on assumed composition and temperature (Lewis, 1969; Weidenschilling and Lewis, 1973; Atreya and Romani, 1985; Carlson et al., 1987; Banfield et al., 1998; Atreya et al., 1999; Irwin, 1999; de Pater et al., 2001). Using revised solar abundances tabulated by Grevesse et al. (2007) in the equilibrium cloud condensation model of Atreya and Romani (1985) and Atreya et al. (1999), cloud bases for solar abundances of oxygen, nitrogen, and sulfur would occur for H_2O at 4.0 bar, for NH_4SH at 1.7 bar, and for NH_3 at 0.54 bar. Galileo Probe Mass Spectrometer measurements and other arguments suggest that Jupiter may have about 4 times the solar abundance of condensable volatiles (Wong et al., 2008). In this case, the H_2O cloud base would be at 5.8 bar, NH_4SH would be at 2.1 bar, and NH_3 would be at 0.67 bar.[4]

* Corresponding author. Fax: +1 650 859 6196.
E-mail address: ksk@sri.com (K.S. Kalogerakis).
[1] Present address: Department of Chemistry, Princeton University, Princeton, NJ 08544, USA.
[2] Present address: Department of Earth, Atmospheric, and Planetary Sciences, Massachusetts Institute of Technology, Cambridge, MA 02139, USA.
[3] Present address: Department of Physics and Astronomy, Michigan State University, East Lansing, MI 48824-2320, USA.

[4] These equilibrium cloud condensation models apply to a moist-adiabatic atmosphere, but are sensitive to the assumed upper boundary temperature. Cloud base values stated above correspond to a temperature structure that achieves 128 K at 400 mbar. For a cooler profile that reaches 123 K at 400 mbar, cloud

0019-1035/$ – see front matter
doi:10.1016/j.icarus.2008.03.001

Recent spectroscopic analyses of Jupiter's atmosphere have found clouds within the pressure ranges expected for ammonia condensation based on the thermodynamic arguments above. For instance, clouds at 0.75 ± 0.20 bar were found by analysis of Galileo imaging (Banfield et al., 1998; Simon-Miller et al., 2001), and thick clouds at 0.90 ± 0.05 bar were retrieved from Cassini CIRS data (Matcheva et al., 2005). These and earlier results (Gierasch et al., 1986) demonstrate that clouds form at the approximate pressure levels expected for ammonia condensation. However, the picture is complicated by Galileo NIMS retrievals indicating cloud *tops* near 1 bar, which can be consistent with ammonia condensation only if the temperature profile were 9 K colder than is commonly accepted, or if Jupiter's deep ammonia abundance were three times greater than was measured by the Galileo Probe (Irwin et al., 2005, 2006). Spectroscopic identification of ammonia ice would naturally be expected to resolve whether an ammonia cloud deck is truly present on Jupiter, but spectroscopic searches did not claim success until the past decade.

Ammonia ices exhibit four fundamental vibrational modes at frequencies of 1057, 1650, 3210, and 3374 cm^{-1}, slightly shifted from their values for the gas-phase ammonia molecule: 932, 1628, 3336, and 3414 cm^{-1} (Fink and Sill, 1982). These four modes correspond to the ν_2 symmetric bend, the ν_4 asymmetric bend, the ν_1 symmetric stretch, and the ν_3 asymmetric stretch, respectively. Several translational and torsional lattice modes are also active in ammonia ices at frequencies below 600 cm^{-1}, and a large variety of combination modes are found throughout the infrared frequency range (Ferraro et al., 1980; Fink and Sill, 1982). The three most intense infrared absorption bands in ammonia ices are associated with the ν_3 mode, the ν_2 mode, and a torsional lattice vibration centered at 363 cm^{-1} (Ferraro et al., 1980; Fink and Sill, 1982). These three absorption features are found in the wavelength regions around 3, 9, and 27 μm, respectively, and we use these wavelength designations throughout the text.

Brooke et al. (1998) observed an anomalous absorption they attributed to ammonia condensates in the 3-μm range in spectra obtained by the Infrared Space Observatory (ISO). Irwin et al. (2001) have pointed out that while the inference of large ammonia particles would give a good fit in the 3-μm range, such particles would introduce unobserved features near 2 and 5 μm by the Galileo Near-Infrared Mapping Spectrometer (NIMS), and the longer wavelengths studied by the Voyager Infrared Interferometer Spectrometer (IRIS). Baines et al. (2002) reported the spectroscopic detection of discrete ammonia ice clouds in data obtained by the Galileo Near-Infrared Mapping Spectrometer (NIMS). Finally, Wong et al. (2004) identified 9-μm absorption signatures in data obtained by the Cassini Composite Infrared Spectrometer (CIRS) during its Jupiter flyby in December 2000. The absorption feature near 27 μm has never been detected in Jupiter's atmosphere. At this wavelength, the transmission weighting function peaks between 300 and 500 mbar. Large (10-μm radius) cloud particles are thought to reside much deeper in the atmosphere, so only smaller (0.5-μm radius) haze particles should be present at the pressure levels sounded at 27 μm (e.g., West et al., 2004). However, the extinction efficiency of 0.5-μm particles at 27 μm is more than two orders of magnitude smaller than at 3 μm, making these haze particles practically invisible to 27-μm radiation.

Baines et al. (2002) reported good agreement between the location of the observed cloud signatures and the regions of condensation predicted by a Rossby wave model of 5-μm hot spots (Friedson and Orton, 1999). They also estimated constraints on the size, lifetime, and spatial distribution of these spectrally identifiable ammonia clouds (SIAC). SIAC were found to occupy only a very small fraction (less than 1%) of Jupiter's surface. This was a rather surprising observation given that, according to the thermochemical equilibrium models for Jupiter, ammonia ice clouds should be ubiquitous. Finally, SIAC appeared most commonly in the northern equatorial region and the Great Red Spot turbulent wake, associating these clouds with areas of strong vertical transport. Baines et al. (2002) placed constraints on the lifetime of SIAC; the clouds were newly formed with lifetimes of approximately one day (mean particle lifetimes range from 0.57 ± 0.32 to 0.97 ± 0.55 days depending on the phase speed of the cloud-generating planetary wave). The largest SIAC detected by NIMS was observed in the turbulent wake region of Jupiter's Great Red Spot. Recent observations by instruments aboard the New Horizons spacecraft also indicate short-lived ammonia clouds with lifetimes of 40 h or less in regions of strong atmospheric upwelling (Reuter et al., 2007).

The spectral features of ammonia ice clouds are expected to have some dependence on the shape and size distributions of the ice particles; larger or irregular particles produce broader absorption signatures, whereas smaller ones have sharper absorption lines (Huffman, 1975). Specifically in the case of ammonia, West et al. (1989) performed discrete dipole calculations for tetrahedral ammonia particles and found that for non-spherical particles the IR spectra can deviate from Mie theory and that the extinction cross-sections in the 9- and 27-μm regions depend on particle shape. They also showed that heterogeneously condensed ammonia ice crystals with non-absorbing cores have reduced extinction cross-sections in the resonance regions.

Clapp and Miller (1993) performed spectroscopic experiments in the infrared studying ammonia aerosols at 111 K. They found that effects related to particle shape influence the position of the absorbance peak in agreement with discrete-dipole approximation calculations. They concluded that a range of particle sizes could dilute the 9-μm absorption feature and affect the uncertainty in the retrieval of ammonia from remote sensing observations. However, as the spectra they collected show, this is only a limited partial effect that could not explain the observed scarcity of ammonia spectral signatures in Jupiter. Detailed modeling of 10-μm CIRS spectra by Wong et al. (2004) required both a thin cloud of small ammonia ice particles (but only in some specific areas) as well as a lower, more optically thick cloud of gray particles.

bases (for H_2O, NH_4SH, and NH_3, respectively) shift to slightly deeper pressures: 4.6, 1.9, and 0.63 bar for 1 × solar abundances, or 6.5, 2.3, and 0.74 bar for 4 × solar abundances (Wong et al., 2008).

The appearance of ammonia clouds in turbulent regions suggests that the nascent ammonia clouds easily undergo some type of processing that modifies their spectroscopic properties. Baines et al. (2002) identified two possible processes: (1) coating of ammonia particles by other substances produced in Jupiter's stratospheric haze (Smith and Tomasko, 1984; Tomasko et al., 1984) and (2) photochemical solid state chemistry ("tanning"), which has also been suggested previously in the context of Uranus (Pollack et al., 1987) and Neptune (Baines and Smith, 1990).

Aerosols are known to decrease Jupiter's geometric albedo in the ultraviolet region of the electromagnetic spectrum (Axel, 1972). Stratospheric haze is optically thin at low and middle latitudes but becomes optically thick near the poles (Tomasko et al., 1986; Rages et al., 1999). Photochemistry and auroral processing of methane have been suggested as sources of the jovian stratospheric haze (Strobel, 1973; Pryor and Hord, 1991). Several models for chemical formation and microphysical properties of stratospheric haze have been proposed (Pryor and Hord, 1991; Moreno, 1996; Banfield et al., 1998; Friedson et al., 2002; Wong et al., 2000; Wong et al., 2003). Atreya et al. (2005) estimated haze production and precipitation rates for both polycyclic aromatic hydrocarbons and hydrazine ice (created by ammonia photolysis and then condensation). They argued that haze precipitation is significant and could thus be a likely reason for the rarity of ammonia ice spectral signatures on Jupiter.

In this paper, we explore the coating hypothesis for masking NH_3-ice spectral features and report laboratory studies and modeling calculations that address the infrared optical properties of ammonia ices coated with hydrocarbons. We perform grazing-angle reflection-absorption infrared (RAIR) spectroscopy on thin ammonia ice films to explore the effects of hydrocarbon coatings on the strong 3- and 9-μm ammonia absorptions. We use multilayer thin film optics computations to interpret our experimental results, revealing the important role of optical interference in altering the ammonia spectral features. Mie scattering calculations confirm that analogous interference effects appear in the predicted spectral signatures of hydrocarbon-coated ammonia ice particles. Several computational examples using Mie and T-matrix models are presented comparing the relative effects of coating thickness, particle size, and particle shape on the single-scattering albedo and extinction efficiency of representative ammonia ice particles.

2. Experiment

An experimental spectroscopic study using thin ammonia ice films allows for a test of the coating and masking hypothesis using controlled conditions with an established technique that is considerably more tractable than working with micro-scale ammonia ice particles.

Spectroscopic characterization of bare and hydrocarbon-coated ammonia ice was performed in a cryogenic apparatus designed for studies of bulk and thin-film materials deposited from the vapor phase. The apparatus consists of a high-vacuum chamber equipped with two independent cryostats: a helium refrigerator capable of reaching 10 K and a liquid-helium-cooled cold finger capable of reaching 4 K. Both cryostats have built-in heaters that allow for controlled cooling and warming rates as well as stable operation over a range of temperatures relevant to those encountered in Jupiter's ammonia clouds and the outer Solar System icy satellites (50 to 150 K).

The vacuum chamber is evacuated using a turbomolecular pump and is fit with multiple ports for diagnostic access and gas introduction. The chamber pressure is monitored using ion gauges and the flow of gases into the chamber is regulated using calibrated leak valves, allowing controlled film deposition rates onto a cryogenically cooled gold mirror (the rest of the vacuum system is at room temperature). Hydrocarbons are maintained in a low-temperature bath before introduction into the chamber. To ensure homogeneous film deposition, gases are introduced through an inlet with no direct line-of-sight to the gold mirror. In this way, molecules undergo a number of randomizing collisions with chamber surfaces before striking the cold mirror face.

Grazing-angle RAIR spectroscopy of the deposited films is performed using a Nicolet Magna-IR 760 FTIR spectrometer with an external MCT-A detector covering the spectral range from 600 to 11700 cm^{-1} (0.85 to 16.7 μm). This spectral range allows us to observe the main absorption features of ammonia near 3 and 9 μm, as well as those of the hydrocarbons used to coat the ammonia ice films. The IR beam from the FTIR spectrometer enters and exits the vacuum chamber through KRS-5 windows and is finally focused on the external MCT-A detector. Inside the vacuum chamber, it reflects off of the cryogenically cooled gold mirror face at an incident angle of 86.0°. Grazing-angle incidence allows for a longer path length of radiation interacting with the thin ice film and thus produces stronger absorption signals. The spectrometer and enclosed beam path are continuously purged with nitrogen gas and kept in a desiccated state. The acquisition of reflected intensity spectra with excellent values of signal-to-noise ratio can be completed in a period of a few seconds to about 1 minute, depending on the spectral resolution and the number of scans averaged.

A relatively high-quality vacuum is needed for these experiments because, in the presence of significant residual water contamination in the chamber, ammonia will form hydrates that give rise to strong broad absorption features near the ammonia absorption features of interest (Bertie and Morrison, 1980; Sill et al., 1981; Moore et al., 2007). The growth of a water ice film on the mirror from residual water contamination was checked by monitoring the broad water ice absorption feature in the 2.86–3.33 μm region (Horn et al., 1995; Teolis et al., 2007) and found to be negligible during the timescale of the experiments.

Although our main experimental conclusions do not depend sensitively on ice film thickness, a measure of the thickness and growth rate of deposited ice layers is needed in order to quantify the magnitude of the effects we observe and for comparisons with Jupiter and the lifetime of its SIAC, as inferred from observations. We estimate the thickness of ice films by the comparison of 3- and 9-μm ammonia absorbance features measured at various times during deposition with simulated

thin-film spectra for layers of different thicknesses (see discussion of optical modeling in following section). Film thicknesses at long deposition times can also be determined from the peak wavelengths of interference fringes appearing below 2.5 μm in both experimental and simulated spectra. The former method is most sensitive for films below ∼100 nm where the magnitude and shape of resonance features change rapidly with film thickness, while the latter method requires ice layers of several hundred nanometers in thickness. The absence of interference fringes at long deposition times can be used to set upper limits on film thickness. Good consistency was found between these two spectroscopic methods of ice thickness determination.

Upper limits for the ice thickness can also be independently estimated by taking into account the molecular collision frequency with the mirror at the gas pressure of deposition, the duration of deposition, and by assuming a sticking coefficient of 1 and the formation of a homogeneous, fully dense film. For example, deposition of ammonia at a pressure of 1 μTorr would result in approximately 5.3×10^{14} collisions s^{-1} cm^{-2} with the cooled substrate. The number of collisions for deposition of benzene at the same pressure is approximately half that for ammonia. At a pressure of 1 μTorr, we estimate upper limits for the deposition rate for ammonia and benzene of ∼10 and ∼5 nm min^{-1}, respectively. Upper limits obtained in this manner for the NH_3 film growth rate were found to be several times larger than values determined by spectral modeling of the 3- and 9-μm absorbance features, a discrepancy that may be due to uncertainties in the value of the NH_3 sticking coefficient, the NH_3 partial pressure, and/or the homogeneity of the thin film layer. Much closer agreement between gas kinetic upper limits and spectral modeling growth estimates were found for benzene coatings.

3. Optical modeling

3.1. Multilayer thin-film reflectance

To simulate the RAIR spectra measured during our coating experiments, we developed a numerical code in JAVA to compute the reflectance of a multilayer thin film as a function of the wavelength, angle of incidence, and polarization of the incident light. The code algorithm is based on a recursive application of the Fresnel equations (Tompkins and McGahan 1999) which describe the transmission and reflection of an electromagnetic plane wave incident on a perfect plane interface separating two optically distinct materials (Yeh, 1998). Each layer is described independently by its thickness and complex wavelength-dependent refractive index, $m = n - ik$. The code was checked extensively against examples found in the book by Heavens (1965) and the two monographs of Abelès (1963, 1971), as well as with the predictions of an existing thin film optics code written in FORTRAN and based on an algebraic solution of the Fresnel equations for a 3-layer system (Abelès, 1963, 1971). The JAVA code was applied to model the optical properties of a variety of multilayer ices (typically three-layer gold/ammonia/vacuum or four-layer gold/ammonia/hydrocarbon/vacuum stacks) to simulate the results of the coating deposition experiments. In these calculations, the incident angle was fixed at 86.0° and the computed reflectance values for s- and p-polarized light were averaged since the FTIR light source is non-polarized.

3.2. Ammonia ice particles

Single-scattering calculations for coated and uncoated spherical ammonia particles were made using FORTRAN implementations of the well known and extensively tested Mie scattering codes for homogeneous and coated spheres presented by Bohren and Huffman (1983). Spherical particle sizes are defined by their radius, r_s. For coated spheres, $r_s = r_c + t$, where r_c is the core radius and t is the coating thickness.

Scattering calculations for non-spherical ammonia particles were made using the double-precision T-matrix FORTRAN code of Mishchenko and Travis (1998) for randomly oriented collections of rotationally symmetric particles. The theoretical basis of the T-matrix method is extensively documented in the literature (Mishchenko et al., 2005). We have limited our exploration of non-spherical particles to prolate spheroids, whose shapes and sizes are described by the ratio $a/b < 1$, where a and b are the lengths of the lateral and the rotational semi-axis, respectively; the volume-equivalent sphere radius, r_v, is given by the formula $r_v = (a^2 b)^{1/3}$.

Both the Mie and T-matrix codes compute a variety of absorption and scattering quantities; in the figures presented here we have focused on two dimensionless parameters: the extinction efficiency and the single-scattering albedo. The extinction efficiency is the sum of the scattering and the absorption efficiencies; the single-scattering albedo is the ratio of the scattering efficiency divided by the extinction efficiency. Efficiencies are equivalent to the scattering, absorption, or extinction cross-sections divided by the geometric cross-section of the particle: i.e., πr_s^2 for spheres. For non-spherical particles, the efficiencies are obtained as the averaged scattering, absorption, or extinction cross-sections for a randomly oriented distribution of particles divided by πr_v^2.

3.3. Optical constants

Experimentally measured optical constants are not available in the temperature range of interest in Jupiter's atmosphere (100–160 K) for either gold, ammonia or the hydrocarbons. The following sets of optical constants are used in our calculations: the gold optical constant values of Lynch and Hunter (1985; room temperature, 0.047–9.919 μm), the liquid benzene values listed by Bertie and Keefe (2004; 25 °C, 6200 to 11.5 cm^{-1}), and a Tholin compilation reported by Khare et al. (1984; room temperature, 0.0207–920 μm). The gold values of Lynch and Hunter (1985) were fit and extrapolated to slightly longer wavelengths using a Drude model (Ordal et al., 1983) to cover the spectral range of interest up to 11 μm.

Several published sets of optical constants for solid ammonia were compared: Robertson et al. (1975; ∼190 K, 5300 to 960 cm^{-1}), Roux et al. (1979; 80 K, 3690 to 710 cm^{-1}); Martonchik et al. (1984; 80 K, 71000 to 50 cm^{-1}) and Howett et

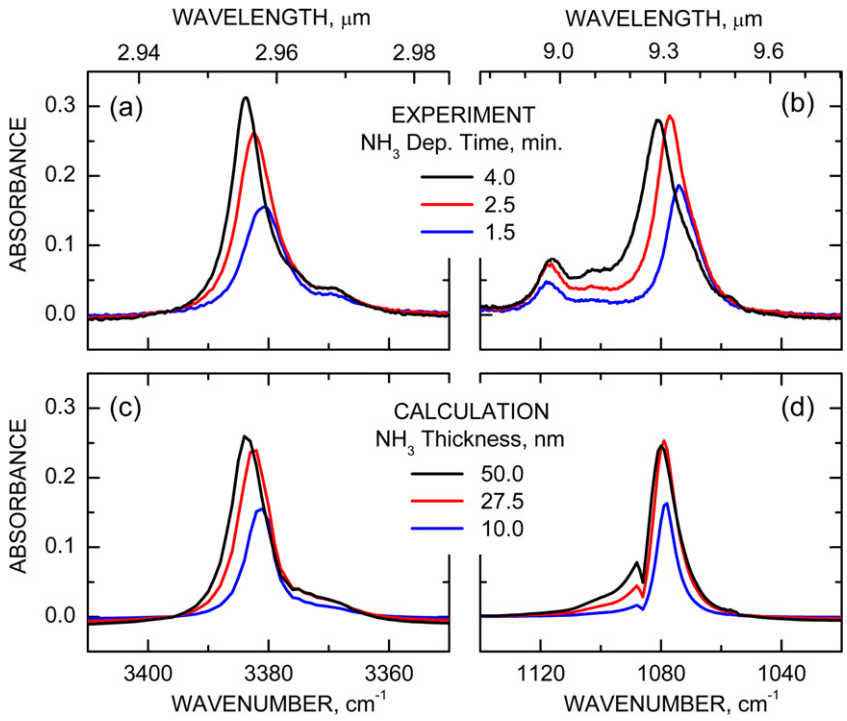

Fig. 1. Reflection-absorption infrared (RAIR) spectra for NH_3 ice deposition for 4 min on a 100 K gold mirror at an average chamber pressure of 6 μTorr: (a) experimental spectrum near 3 μm; (b) experimental spectrum near 9 μm; (c) simulated spectrum near 3 μm; and (d) simulated spectrum near 9 μm. Experimental absorbance spectra are obtained using the formula $-\log(I/I_0)$, where I and I_0 are the reflected light intensity spectra collected with and without a condensed film present.

al. (2007; 80 K, 12000 to 1300 cm^{-1}). The latter authors have also provided an unpublished data set containing preliminary measurements extending further into the infrared to 1000 cm^{-1}. Each tabulated set of optical constants was stored as a function of wavenumber and interpolated linearly for reflectance and scattering calculations performed with 1-cm^{-1} resolution. We refer to these sets of optical constants below by the name of each study's first author.

Differences between the temperature of available experimental optical constant datasets and the conditions of our measurements undoubtedly influence the agreement between experimental and simulated RAIR spectra. A similar uncertainty exists in cloud simulations used to interpret optical measurements of the jovian atmosphere. For quantitative comparisons of our experimental results and the detection of subtle changes, sets of optical constants for ammonia and various hydrocarbons at 100 K are desirable, and we plan such measurements in the future. Nevertheless, in the present work, the coating hypothesis is explored by looking for significant changes in the two strong ammonia absorption features at 3 and 9 μm, and the limitations of the available optical constant data sets are not critical to the central conclusions of this study.

4. Experimental results and simulations of thin film absorbance

The absorbance observed experimentally is a function of ice properties, wavelength, and other experimental conditions, such as the angle of incidence, the light polarization, and the optical properties of the mirror. Thus, it includes all absorption, scattering, and interference contributions. The experimental absorbance spectra are obtained using the formula $-\log(I/I_0)$, where I and I_0 are the reflected light intensity spectra collected with and without a condensed film present. The simulations take into account all the aforementioned parameters that influence the absorbance in the experiments. Simulated absorbance spectra were obtained using the formula $-\log(R/R_0)$, where R and R_0 are the polarization-averaged reflectance values for the stack and the bare gold substrate, respectively.

Figs. 1a and 1b show the evolution of RAIR spectra near the 3- and 9-μm NH_3 absorption features collected during ammonia ice deposition on a gold mirror at 100 K. Each experimental spectrum is the average of 32 scans taken with a resolution of 0.250 cm^{-1}. Ammonia ice was grown for a total of 4 minutes at an average pressure of about 6 μTorr. The amplitude and area of the primary absorption features increase rapidly during the initial phases of ice growth, and begin to saturate at later times.

Figs. 1c and 1d show thin-film optics simulations of the 3- and 9-μm absorbance features using the Roux optical constants for NH_3. The set of ice thicknesses is chosen to reproduce the spectral evolution observed in the experiment while remaining roughly proportional to deposition rates estimated from gas kinetics. A conservative estimate for the uncertainty in the thickness of the final NH_3 film (50-nm thickness) after 4 min of deposition is ±15 nm.

The Roux optical constants provide the best overall simulations for the evolution of the 3- and 9-μm features in our thin film computations, in particular, reproducing the simultaneous saturation of the 9-μm feature and growth of the 3-μm features observed in the experimental spectra at 2.5 and 4 min.

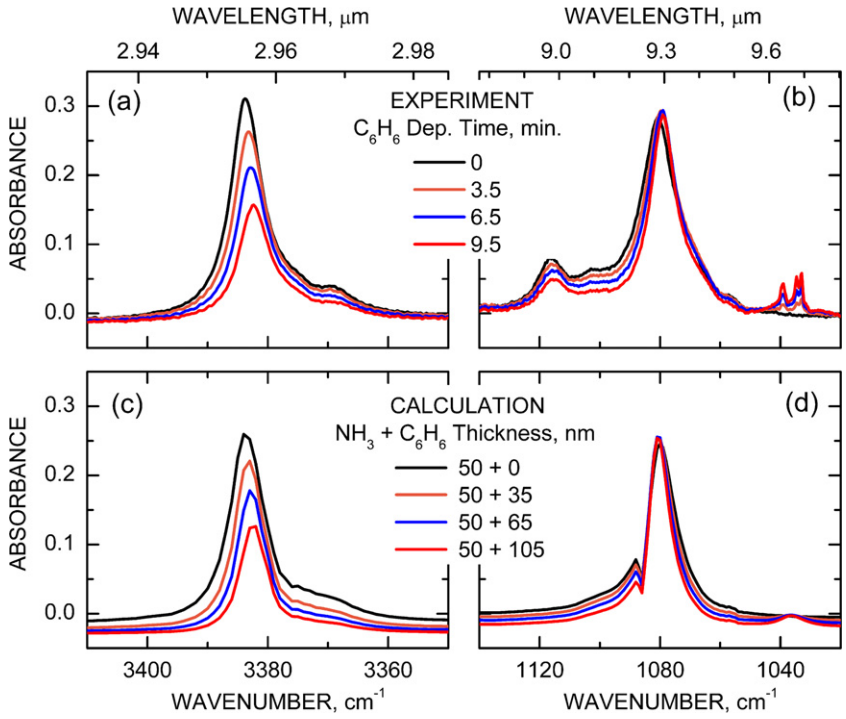

Fig. 2. RAIR spectra for benzene deposition on an NH_3 ice film at 100 K for 9 minutes at an average chamber pressure of 2.5 μTorr: (a) experimental spectrum near 3 μm; (b) experimental spectrum near 9 μm; (c) simulated spectrum near 3 μm; and (d) simulated spectrum near 9 μm.

The Robertson set (Robertson et al., 1975) produces unacceptable simulations of the 3-μm feature and is not considered further. The Howett constants (Howett et al., 2007) reproduce the 3-μm feature in a very similar manner to the Roux constants, while the Martonchik constants (Martonchik et al., 1984) lead to a broader asymmetric 3-μm feature that is a less satisfactory match to experiment. Clapp and Miller (1993) have similarly found that Mie scattering calculations using the Martonchik constants provide a less satisfactory fit to experimental aerosol spectra near 9 μm than those using the Roux constants.

However, it should be noted that none of the optical constant datasets fully capture the observed spectral shapes and their absolute magnitudes, probably because of the temperature difference between our experiments (100 K) and the optical constant measurements (80 K). This discrepancy is likely to cause deviations in the calculated absorption features related to the mixture of phases and microstructures present in the NH_3 ice (Holt et al., 2004; Dawes et al., 2007). Nevertheless, with the exception of the Robertson set, all the available sets of optical constants used yield the same conclusions as far as the scope of the present study is concerned.

The smaller absorption peak located near 1115 cm^{-1} in Fig. 1b is not reproduced in any of the thin film simulations, suggesting that its origin is not pure solid ammonia. A very strong absorption band at this wavenumber has been reported for ammonia dihydrate, however other very strong bands expected near 3404, 3396, 3391, 3207, 3150, and 900 cm^{-1} are all absent in our spectra. The 1115 cm^{-1} absorption feature is not associated with either ammonia monohydrate or hemihydrate (Bertie and Morrison, 1980; Moore et al., 2007), and remains unidentified.

After growth of the ammonia ice film to an approximate thickness of 50 nm, the NH_3 flow is interrupted and benzene is deposited at an average pressure of about 2.5 μTorr for a total time of approximately 9.5 min. Figs. 2a and 2b show the experimental RAIR spectra collected during benzene deposition. As the benzene condenses on top of the ammonia ice and the coating grows thicker, the ammonia absorbance peak in Fig. 2a is steadily reduced in magnitude. Clearly, this brief benzene exposure partially suppresses the 3-μm NH_3 absorbance feature. Fig. 2b shows that while benzene deposition somewhat diminishes the shoulder of the 9-μm absorbance feature, the main peak remains relatively unchanged by the benzene coating. In Fig. 2b, we also note the gradual appearance of the fundamental ν_{14} vibrational mode of benzene near ∼1035 cm^{-1} as the coating grows thicker (Bertie and Keefe, 2004).

What is remarkable in the data shown in Figs. 2a and 2b is that benzene is essentially transparent in these wavelength regions (Bertie and Keefe, 2004), but is nevertheless effective at reducing or partially masking the 3-μm ammonia absorbance feature. Given the rather inert nature of hydrocarbons, and the low temperatures and short times of the experiment, chemical reactivity is not a likely cause for this effect. A more plausible hypothesis for the observed behavior is optical interference.

Figs. 2c and 2d show thin film optics simulations for a 50-nm NH_3 ice layer coated with 35, 65, and 105 nm of benzene ice. The simulations reproduce the general trends we observed in the experimental RAIR spectra. The fact that thin film optics computations can simultaneously replicate the masking of the 3-μm feature and the insensitivity of the 9-μm peak height with increasing the benzene thickness strongly supports optical in-

terference effects as the dominant mechanism responsible for our experimental observations. The simulations do not reproduce the strength or structure of the benzene ν_{14} absorbance feature very well, suggesting that the available optical constant set for *liquid* benzene at room temperature does have some limitations when applied to benzene *ice* at 100 K.

We note that benzene coating also depresses other less prominent ammonia absorbance features like the ν_4 asymmetric bend near 6.1 μm and its first overtone $2\nu_4$ just to the red of the large ν_3 feature, as well as the weak $\nu_2 + \nu_3$ and $\nu_3 + \nu_4$ combination bands near 2.2 and 2.0 μm.

The real refractive index n of liquid benzene at room temperature lies in the range 1.47–1.50 in both wavelength regions of interest. The imaginary refractive index k has a value less than 10^{-4} near the 9-μm ammonia absorption and less than 0.04 near the 3-μm absorption (Bertie and Keefe, 2004). To test the dependence of the masking effect on the refractive index of the coating, spectral simulations were computed for ammonia ice covered by hypothetical non-absorbing coatings ($k = 0$) with different refractive indices ranging from $n = 1$ to 1.7, the typical range associated with hydrocarbons in the infrared. Simulations with $n = 1.5$ are essentially indistinguishable from those for benzene. We find that the masking effect at the 3-μm ammonia absorbance feature strengthens as the refractive index of the coating increases, while the peak height of the 9-μm feature remains relatively unchanged. This difference is a consequence of the respective combinations of wavelength, ice film thickness, and refractive index values.

These spectral simulations are consistent with the effects on ammonia absorbance features we observed in other experiments with various different hydrocarbon coatings, including mixtures of aliphatic hydrocarbons (mixtures with butane to octane and nonane to dodecane), mixtures of aromatic hydrocarbons (benzene, toluene, ethylbenzene, and xylene), and single compounds such as benzene, hexane, and cyclohexane. In all these cases, the suppression of the 3-μm ammonia absorbance feature scales with the respective hydrocarbon's refractive index.

Fig. 3 shows the effect of prototypical simple aliphatic (hexane), cyclic (cyclohexane), and aromatic (benzene) hydrocarbon coatings on the magnitude of the 3-μm absorbance feature of a 50-nm thick ammonia ice film. The hydrocarbon coating thickness values shown in Fig. 3 are computed from measured pressures, deposition times, and gas kinetic relations assuming unity sticking coefficients. For benzene and cyclohexane, these gas-kinetic coating thicknesses are consistent with estimates based on the appearance of interference fringes in the final experimental RAIR spectra collected during hydrocarbon deposition. For hexane, no fringes appeared even at the longest deposition times, so the final thickness of 300 nm is only an upper limit and true film thicknesses may be systematically smaller. Fig. 3 also plots thin film computations for non-absorbing coatings with $n = 1.2$, 1.4, and 1.6. The infrared optical constants of solid or liquid cyclohexane and hexane were not found in the literature, however at visible wavelengths, the real refractive indices of liquid cyclohexane and hexane are approximately 1.42 and 1.37, respectively (Aminabhavi et al., 1996). Neither liquid hydrocarbon has strong absorption features that overlap with the 3-μm NH_3 absorption feature (Szymanski, 1964).

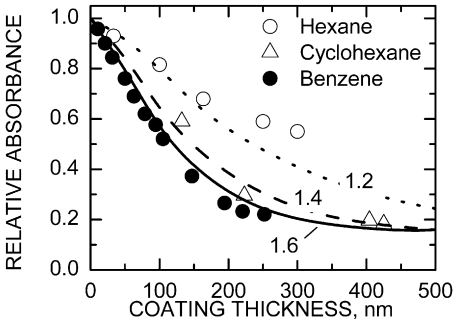

Fig. 3. Effect of different hydrocarbon coatings on the 3-μm absorbance feature of a 50-nm thick ammonia ice film at 100 K; the symbols represent experimental data points and the lines the results of thin film optical computations. The relative absorbance of the coated NH_3 film is calculated as the baseline-corrected magnitude of the 3-μm absorbance feature divided by the baseline-corrected absorbance magnitude at zero coating thickness.

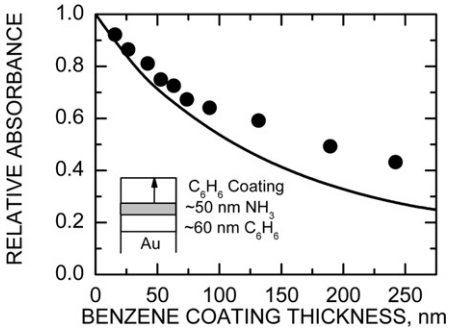

Fig. 4. Effect of a benzene coating on the magnitude of the 3-μm absorbance feature of a ∼50 nm ammonia ice film deposited on top of a ∼ 60 nm benzene ice film: the solid circles represent experimental data points at 100 K and the solid line the result of thin film optical computations.

A variety of measurements were also conducted on mixed ices formed by the co-deposition of ammonia with various hydrocarbons, and on composite ices formed by the sequential deposition of ammonia and hydrocarbon layers. An example of the latter is shown in Fig. 4, for a benzene–ammonia–benzene multilayer ice film. Experimental benzene ice thicknesses are computed from gas kinetic relations and are consistent with the values obtained from spectral simulation. The intermediate ammonia ice layer thickness of ∼50 nm is estimated by comparison of the calculated and experimental 3-μm absorbance feature; this spectrally derived thickness is about half of the gas kinetic value. A similar reduction in the strength of the 3-μm ammonia absorbance feature with benzene coating is observed experimentally and reproduced computationally for the composite film as for the single films of Figs. 2 and 3. Agreement between experiment and computation is satisfactory considering the uncertainty in the thicknesses of the different ice layers and the fact that none of the optical constants used in the computation have been measured at the temperature of the experiments.

5. Ammonia particle simulations

The existence and strength of analogous interference effects for hydrocarbon coatings on ammonia ice particles can be assessed using Mie scattering computations. Since the details of ammonia particle size and shape distributions in the jovian clouds are still highly uncertain and our calculations are only illustrative, we limit our calculations to the single-particle properties of ammonia ice particles with effective radii of 1 and 10 μm. These choices are motivated by several published studies. A recent review of jovian cloud and haze research concludes that retrieved mean particle radii in the upper tropospheric haze are typically around 0.5 μm, while deeper in the atmosphere particle sizes increase to several microns, with a mean radius of around 10 μm where ammonia ice spectra are detected (West et al., 2004). Detailed modeling of the CIRS spectrum near the 9-μm ammonia absorption feature by Wong et al. (2004) concluded that observations are best reproduced by a two-cloud model wherein one cloud particle population has radii near 1 μm and the other near 10 μm. A similar bimodal ammonia particle size distribution provided the best scattering model for the ISO 3-μm reflection spectrum of Jupiter (Brooke et al., 1998).

Fig. 5 shows the effect of benzene coatings on the single-scattering albedo and extinction efficiency of 1-μm radius ammonia spheres in the 3- and 9-μm spectral regions. Similar Mie scattering computations are presented for 10-μm ammonia spheres in Fig. 6. The benzene coating increments in Figs. 5 and 6 amount to 10 and 100% of the ammonia sphere radius; intermediate coating thickness values produce intermediate effects. In general, a benzene coating thickness of 10% of the ammonia particle radius makes only minimal changes to the optical properties. The most notable change is the loss of the sharp albedo features for the 10-μm particle in Figs. 6a and 6b. This loss is particularly prominent near 9 μm where the albedo increases from ∼0.2 to 0.6, with a similarly large increase in the extinction efficiency. However, these changes are limited to a relatively narrow spectral range and for the entire wavelength region as a whole the effect of benzene coating is moderate.

Benzene coatings of the same thickness as the particle radius have a large impact on the computed optical properties for both particles and both wavelength regions. For the smaller 1-μm particle, the coating essentially removes the sharp albedo feature in the 3-μm region (Fig. 5a), and greatly increases the extinction efficiency (Fig. 5c). In the 9-μm region, the broad low-albedo feature is dramatically narrowed and red-shifted; the albedo at 9 μm increases from less than 0.1 to greater than 0.9 (Fig. 5b), and the extinction efficiency maximum near 9.4 μm falls by a factor of 3 (Fig. 5d).

Less dramatic, but still significant, changes occur for the larger 10-μm particle. The albedo across the entire wavelength region of Fig. 6a is increased, and the sharp minimum near 2.95 μm is gone. Likewise the albedo minimum near 9.1 μm is completely removed and a new minimum appears to the red at about 9.6 μm (Fig. 6b). The extinction efficiency in the 3-μm region is not greatly affected by the thick benzene coating (Fig. 6c), however noticeable changes are seen in the 8–9.5 μm range with decreased extinction below, and increased extinction above, 8.7 μm (Fig. 6d).

Similar computations have been performed using the Howett and Martonchik ammonia optical constants, for both benzene and tholin coatings. While there are differences in the spec-

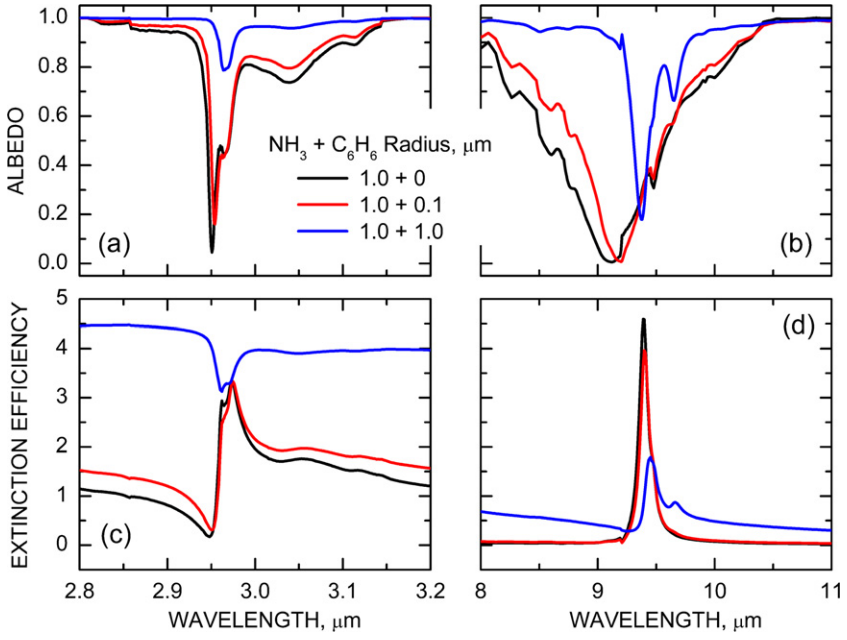

Fig. 5. The effect of benzene coating on Mie scattering properties of a 1 μm radius ammonia sphere: the single-scattering albedo in (a) the 3-μm region and (b) the 9-μm region; the extinction efficiency in (c) the 3-μm region and (d) the 9-μm region. The benzene coating increments are 10 and 100% of the ammonia sphere radius. Simulated absorbance spectra were obtained using the formula $-\log(R/R_0)$, where R and R_0 are the polarization-averaged reflectance values for the stack and the bare gold substrate, respectively. Computations were performed using the same set of optical constants for ammonia (Roux et al., 1979) and benzene (Bertie and Keefe, 2004), as were used for the thin film simulations of Fig. 2.

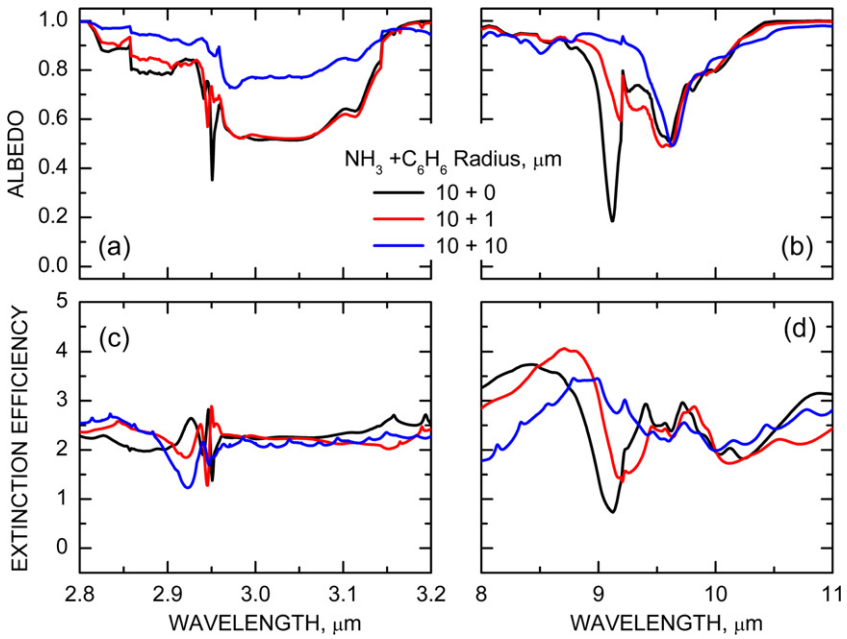

Fig. 6. The effect of benzene coating on Mie scattering properties of a 10-μm radius ammonia sphere: single-scattering albedo in (a) the 3-μm region and (b) the 9-μm region; extinction efficiency in (c) the 3-μm region and (d) the 9-μm region. The benzene coating increments are 10 and 100% of the ammonia sphere radius.

tral shapes of the albedo and extinction efficiencies produced using different combinations of optical constants, the general trends predicted for hydrocarbon coating are very similar; thin coatings ($t = r_c/10$) make minimal changes while thick coatings ($t = r_c$) obscure, and in some cases shift, the sharp minima and maxima associated with the fundamental ammonia absorption features. The main differences between benzene and tholin coatings occur in the shoulder regions of the main 3-μm albedo absorption feature; benzene coatings increase the albedo slightly while tholins coatings decrease the albedo. Similar behavior is seen in the 9-μm region. These differences are likely due to the larger value of the absorption coefficient for tholins with respect to benzene in these spectral regions.

Hydrocarbon coatings can also alter the scattering properties at weaker ammonia absorption features. Fig. 7 shows Mie computations for tholin-coated 1-μm ammonia spheres in the 1.9–2.7 μm spectral region to the blue of the main 3-μm ammonia absorption feature. This spectral region contains various combination band ammonia absorptions (Ferraro et al., 1980) and was recently used by Baines et al., e.g. at 2.0 and 2.7 μm, to identify ammonia ice absorption in Jupiter from *Galileo* Near-Infrared Mapping Spectrometer (NIMS) spectra (Baines et al., 2000, 2002). Computations were performed with the Martonchik optical constants for ammonia because the Roux optical constants do not extend into this spectral region. For the highly reflective 1-μm ammonia particle, the spectral features in the albedo are small (Fig. 7a), while for the 10-μm particle, the minima near the wavelengths 2.0, 2.2, and 2.6 μm (Fig. 7b) are comparable in magnitude to that of 3-μm albedo feature (Fig. 6a). The 10% tholin coating has a larger effect on the 1-μm particle than on the 10-μm particle, noticeably increasing the extinction efficiency (Fig. 7c) and decreasing the albedo contrast (Fig. 7a). A 100% tholin coating makes large changes to the albedo features for both particles. For small particles, the thick tholin coating lowers the extinction efficiency below 2.2 μm and increases it above 2.2 μm (Fig. 7c); for the large particle, the thick coating introduces oscillations into the extinction efficiency around a mean value of about 2 (Fig. 7d).

Coating thickness has an equal or stronger effect on the computed optical parameters than comparable variations in particle size and shape. Figs. 8 and 9 show Mie scattering computations made for pure ammonia particles with the same total sphere radii as the benzene-coated particles in Figs. 5 and 6. As in the case of adding a thin benzene coating, increasing the radius of an ammonia particle by 10% results in minimal changes to computed properties. However, a comparison of Figs. 5 and 8, and Figs. 6 and 9, reveals greater changes to the spectral features by adding a thin benzene coating than by a comparable increase in the ammonia particle size. This is particularly evident for the 10-μm particle, where the 10% increase in particle radius leaves the albedo minima almost unchanged in both Figs. 9a and 9b, whereas a similar increase by benzene coating noticeably alters these features in Figs. 6a and 6b.

Computed properties for a particle with a 100% benzene coating versus a pure ammonia particle with twice the radius are very different. Doubling the particle size does not obscure or move the sharp minima observed in the albedos of pure ammonia particles (Figs. 8a, 8b, 9a, and 9b), whereas a thick benzene coating greatly suppresses and in some cases shifts these minima (Figs. 5a, 5b, 6a, and 6b). Similarly large differences can be observed in the extinction efficiency. For example, benzene coating removes the extinction minimum at ∼2.95 μm and the extinction maximum at ∼9.4 μm for the 1-μm particle in Figs. 5c and 5d, but doubling the pure ammonia particle size does neither in Figs. 8c and 8d. These differences are a result of thin film optics interference and their strong dependence on the relative values of the substrate and coating refractive indices.

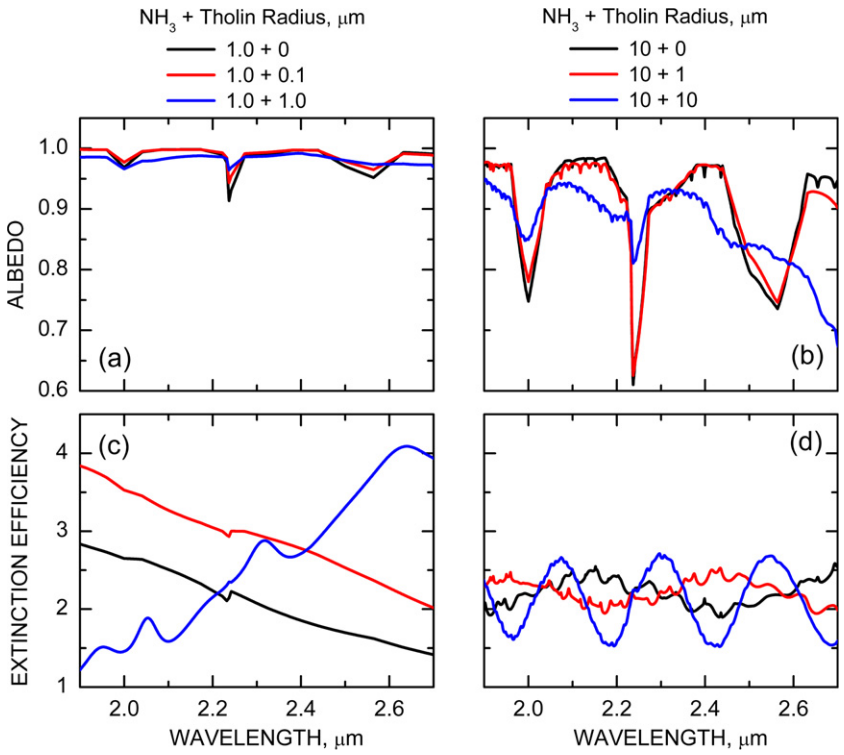

Fig. 7. The effect of tholin coating on the Mie scattering properties of ammonia particles in the 1.9 to 2.7 μm wavelength region: single-scattering albedo for (a) a 1-μm sphere and (b) a 10-μm sphere; extinction efficiency for (c) a 1-μm sphere and (d) a 10-μm sphere. The tholin coating increments are 10 and 100% of the sphere radius.

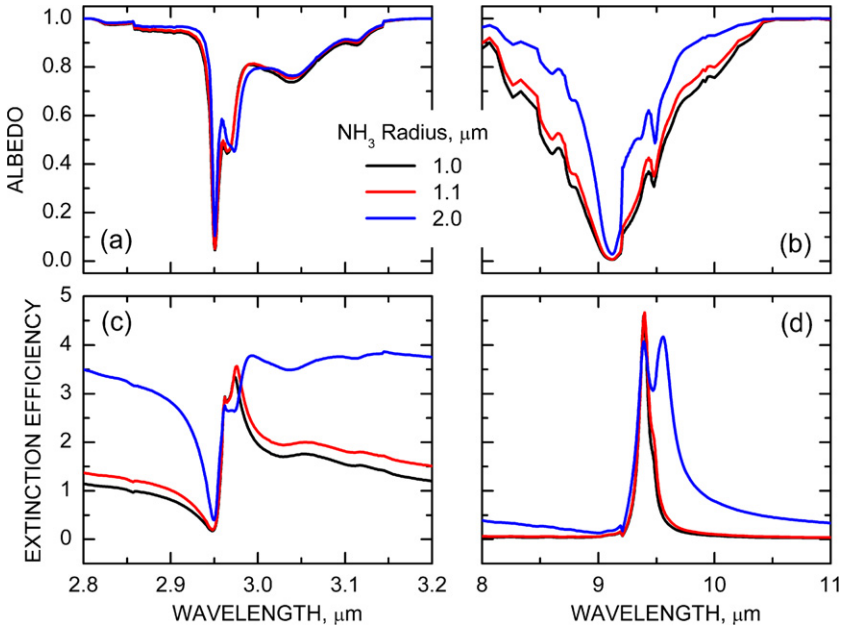

Fig. 8. The effect of size variation on Mie scattering properties of a 1-μm radius ammonia sphere: single-scattering albedo in (a) the 3-μm region and (b) the 9-μm region; extinction efficiency in (c) the 3-μm region and (d) the 9-μm region.

In Fig. 10 we present the effect of particle shape on the scattering properties of small ammonia particles by comparing T-matrix computations for a 1-μm radius sphere to those for prolate spheroids with $a/b = 1/4$ and $r_v = 0.79$ and 1.59 μm. The spheroid with $r_v = 0.79$ μm mimics a linear chain of four spherical 0.5-μm radius particles, a configuration found to best fit laboratory ammonia aerosol spectra and used in a jovian ammonia cloud model to simulate the CIRS spectrum near the 9-μm ammonia absorption feature (Wong et al., 2004). The larger prolate spheroid mimics a linear chain of four 1-μm spheres. The effects of these particle shapes on the magnitudes of albedo features in the 3-μm region are relatively minor, with the largest

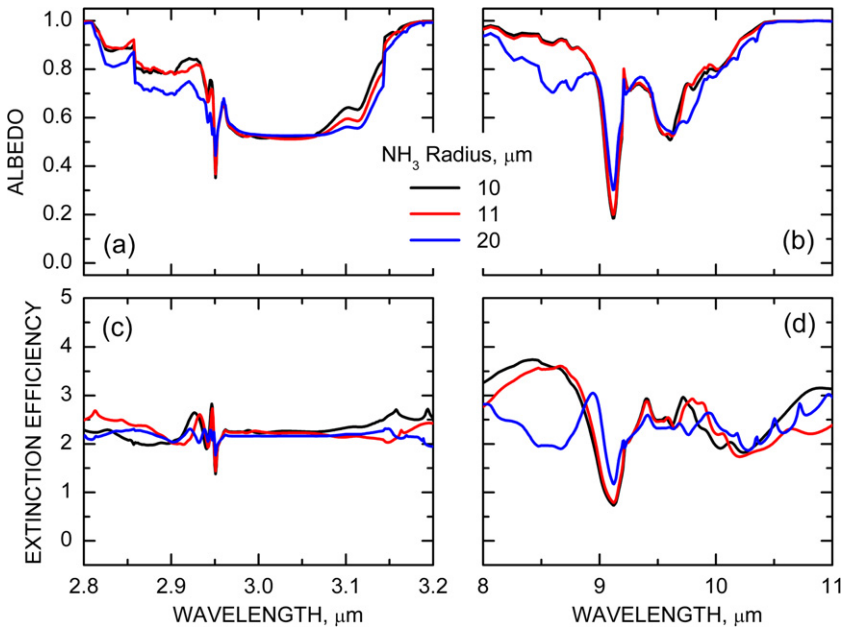

Fig. 9. The effect of size variation on Mie scattering properties of a 10-μm radius ammonia sphere: single-scattering albedo in (a) the 3-μm region and (b) the 9-μm region; extinction efficiency in (c) the 3-μm region and (d) the 9-μm region.

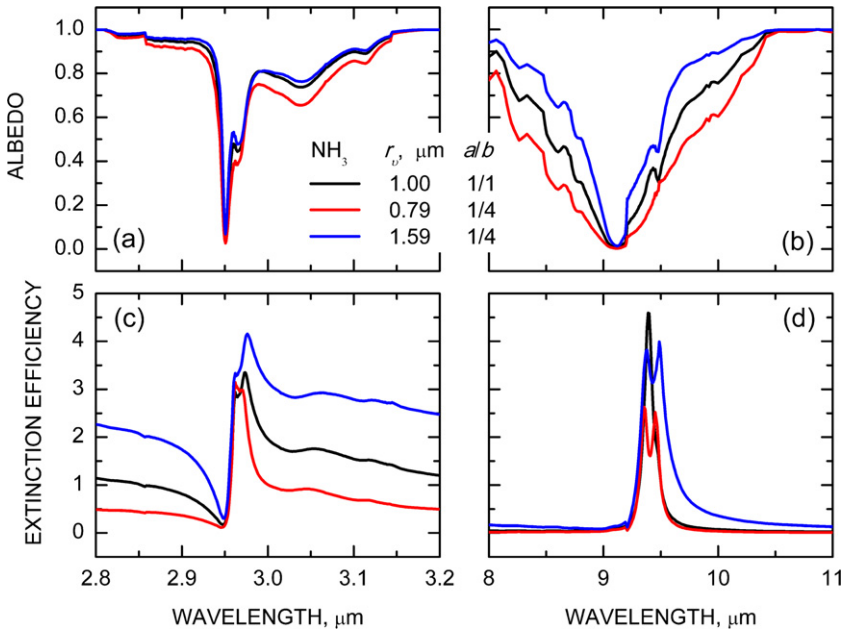

Fig. 10. Effect of particle shape on T-matrix scattering computations for small non-coated ammonia ice particles: (a) the 3-μm region and (b) the 9-μm region.

relative changes occurring on the red shoulder of the main absorption feature (Fig. 10a). In the 9-μm region, particle shape plays a much more significant role, narrowing or broadening the main albedo minimum (Fig. 10b). However, in both wavelength regions the spectral locations and the magnitudes of the albedo minima do not differ with particle shape. Similarly, the extinction minimum in the 3-μm region (Fig. 10c) and the extinction maxima in the 9-μm region (Fig. 10d) are not removed going from spherical to these prolate spheroid geometries.

The general conclusion that can be drawn from these simulations is that coating of ammonia particles by hydrocarbons produces different effects on the scattering properties than moderate size or shape changes in pure ammonia particles. In particular, hydrocarbon coating is more effective at reducing or removing sharp features (maxima or minima) associated with the fundamental ammonia absorptions.

6. Discussion and conclusions

In this work we have examined and verified the hypothesis that hydrocarbon coatings can mask the spectral features associated with strong ammonia absorption bands by: (1) experimentally demonstrating the reduction of absorbance features in thin ammonia ice films coated with hydrocarbons, (2) showing the

consistency of these results with thin film optics simulations, and (3) confirming that a similar masking effect is predicted by Mie theory for the scattering properties of hydrocarbon-coated ammonia ice particles.

An important observation is that interference effects can obscure ammonia absorption signatures in both thin-film RAIR spectra and small particle scattering properties, even if the coating itself is transparent. The efficiency of this masking effect increases with increasing real refractive index of the coating. Any overlap between important ammonia absorption bands and those of the coating will obviously lead to additional effects, but such absorption features by the coating are not required to alter the ammonia spectral features. The importance of interference effects in laboratory thin-film RAIR spectroscopy has been highlighted by several researchers, especially in the case of water ice (Horn et al., 1995; Teolis et al., 2007).

Photolysis of methane in Jupiter's atmosphere gives rise to a broad range of hydrocarbons including simpler ones that have been observed, such as ethane, propane, acetylene, and benzene, as well as more complex ones that have been predicted in models but not yet observed (Atreya et al., 2005). Benzene has only recently been detected in Jupiter (Bézard et al., 2001). Obviously, several different hydrocarbon molecules could have a cumulative masking effect. The most abundant hydrocarbons in Jupiter (methane, ethane) are not condensable at the temperature of the jovian ammonia clouds. However, propane and higher hydrocarbons are condensable. Voyager IRIS detected propane in Jupiter and determined an upper limit for the mixing ratio of 6×10^{-7} (Kim et al., 1985). More complicated organic compounds such as polycyclic aromatic hydrocarbons, nitriles, or heterocyclic compounds can also have a more direct masking effect with strong absorption features overlapping or near the ammonia absorption features. Several groups have investigated the thermal, photochemical, and ion irradiation effects on ices (Allamandola et al., 1988; Bohn et al., 1994; Gerakines et al., 1996; Moore and Hudson, 2003). In all cases, a number of new molecules were produced providing important clues on some mechanisms of production of complex organic molecules in these ices. An abundance of such molecules has also been predicted in Jupiter's atmosphere, resulting from auroral activity in the polar regions (Pryor and Hord, 1991; Moreno, 1996; Banfield et al., 1998; Friedson et al., 2002; Wong et al., 2000, 2003).

Pressure on the order of a few μTorr used for benzene deposition on ammonia ice during the experiment shown in Fig. 2 is several hundred times larger than partial pressures consistent with spectroscopic measurements of jovian benzene (Bézard et al., 2001). Given an exposure time of a few minutes in the laboratory experiments, the corresponding equivalent time in Jupiter would be somewhere between one and a few days. This period of time is comparable to estimated spectrally-identifiable ammonia cloud lifetimes in Jupiter (Baines et al., 2002).

While our experiments and optical simulations confirm the existence of a hydrocarbon coating effect on ammonia ice spectral features, the impact of this effect on the detection of ammonia ice clouds in Jupiter is difficult to assess and sensitive to assumptions made about the concentrations of potential coating species and the dynamics of the cloud formation and coating processes.

A uniform coating of hydrocarbons applied to a broad size distribution of ammonia ice particles will have a stronger impact on the spectra of the smallest particles. For example, a 1-μm benzene coating makes a much greater impact on the optical properties of a 1-μm sphere (Fig. 5) than on a 10-μm sphere (Fig. 6). Equivalently, for a constant coating rate, large particles will have a longer "spectral shelf life" than small particles. But in reality, several effects may complicate the simple picture of fixed-size ammonia ice particles residing in the atmosphere while undergoing the coating process.

Actual cloud particles are subject to microphysical processes of condensation, evaporation, coagulation, coalescence, and sedimentation (e.g., Rossow, 1978; Carlson et al., 1988). These processes lead to more complicated interactions between ammonia ice and precipitating hydrocarbons, such as heterogeneous ammonia condensation onto hydrocarbon cores (West et al., 1989), and mixed-particle growth through collisions of previously coated particles. Collisional growth can have an effect similar to accelerated coating rate. For instance, consider a 2-μm particle and three 1-μm particles. If all are coated with a 1-μm layer of hydrocarbons, and the three coated 1-μm ammonia ice particles combine to form a single mixed particle (with about the same volume as the coated 2-μm particle), then the hydrocarbon-to-ammonia volume fraction is about three times larger for the merged particle than for the coated 2-μm particle. Thus, a complete understanding of the influence of coatings on Jupiter's spectrum requires a complete and simultaneous treatment of atmospheric dynamics, cloud formation, and cloud microphysics, an effort that is well beyond the scope of this report.

The focus of this study was on coating by direct condensation of gaseous hydrocarbons onto ammonia ice. Atreya et al. (2005) discussed a related mechanism, in which the coating was formed by a mixture of photochemically produced material. We find that coatings of different compositions provide the same masking effect, suggesting that the Atreya et al. (2005) process, although microphysically distinct from gas-phase condensation onto ammonia ices, could nonetheless provide similar spectral masking effects.

The main conclusions of this work are that experiment and modeling support a masking effect of hydrocarbon films on ammonia absorption features, and that the inference of the coating hypothesis for the absence of strong ammonia cloud spectral signatures in Jupiter cannot be dismissed. As our understanding of the composition of Jupiter's atmosphere evolves, it will be possible to progressively obtain more accurate estimates of the composition and amount of available condensable matter that could coat ammonia ice particles. Accurate measurements of optical constants for ammonia and hydrocarbon species at the appropriate temperature ranges are also needed, particularly to identify the subtle changes in spectral features that might allow the separation of particle size and shape effects from those of hydrocarbon coating in observational data.

Acknowledgments

We gratefully acknowledge financial support from the NASA Outer Planets Research Program under Grant NNG06GF37G and from the NSF Planetary Astronomy Program under Grant AST-0206270. The participation of Rhiannon T. Meharchand, Patricia A. Engel, and Anand U. Oza was made possible by the NSF Research Experiences for Undergraduates Program under Grant PHY-0353745. We also thank James E. Boulter and Christina E. Baer for their help in the early stages of the project, our colleagues at SRI's Molecular Physics Laboratory for helpful advice and discussions, and Kevin H. Baines and Patrick G.J. Irwin for their careful reading of the manuscript and insightful comments.

References

Abelès, F., 1963. Methods for determining optical parameters of thin films. In: Wolf, E. (Ed.), Progress in Optics. Wiley, New York, pp. 251–288.

Abelès, F., 1971. Optical properties of metallic films. In: Francombe, M.H., Hoffman, R.W. (Eds.), Physics of Thin Films. Academic Press, New York, pp. 151–204.

Allamandola, L.J., Sandford, S.A., Valero, G.J., 1988. Photochemical and thermal evolution of interstellar/precometary ice analogs. Icarus 76, 225–252.

Aminabhavi, T.M., Patil, V.B., Aralaguppi, M.I., Phayde, H.T.S., 1996. Density, viscosity, and refractive index of the binary mixtures of cyclohexane with hexane, heptane, octane, nonane, and decane at (298.15, 303.15, and 308.15) K. J. Chem. Eng. Data 41, 521–525.

Atreya, S.K., Romani, P.N., 1985. Photochemistry and clouds of Jupiter, Saturn, and Uranus. In: Hunt, G.E. (Ed.), Recent Advances in Planetary Meteorology. Cambridge Univ. Press, Cambridge, pp. 17–68.

Atreya, S.K., Wong, M.H., Owen, T.C., Mahaffy, P.R., Niemann, H.B., de Pater, I., Drossart, P., Encrenaz, T., 1999. A comparison of the atmospheres of Jupiter and Saturn: Deep atmospheric composition, cloud structure, vertical mixing, and origin. Planet. Space Sci. 47, 1243–1262.

Atreya, S.K., Wong, A.S., Baines, K.H., Wong, M.H., Owen, T.C., 2005. Jupiter's ammonia clouds—Localized or ubiquitous? Planet. Space Sci. 53, 498–507.

Axel, L., 1972. Inhomogeneous models of the atmosphere of Jupiter. Astrophys. J. 173, 451–468.

Baines, K.H., Smith, W.H., 1990. The atmospheric structure and dynamical properties of Neptune derived from ground-based and IUE spectrophotometry. Icarus 85, 65–108.

Baines, K.H., Carlson, R.W., Kamp, L.W., 2000. Spectral detection of ammonia ice in the turbulent clouds of Jupiter by Galileo/NIMS. Bull. Am. Astron. Soc. 32, 997.

Baines, K.H., Carlson, R.W., Kamp, L.W., 2002. Fresh ammonia ice clouds in Jupiter. I. Spectroscopic identification, spatial distribution, and dynamical implications. Icarus 159, 74–94.

Banfield, D., Gierasch, P.J., Bell, M., Ustinov, E., Ingersoll, A.P., Vasavada, A.R., West, R.A., Belton, M.J.S., 1998. Jupiter's cloud structure from Galileo imaging data. Icarus 135, 230–250.

Bertie, J.E., Keefe, C.D., 2004. Infrared intensities of liquids XXIV: Optical constants of liquid benzene-h_6 at 25 °C extended to 11.5 cm^{-1} and molar polarizabilites and integrated intensities of benzene-h_6 between 6200 and 11.5 cm^{-1}. J. Mol. Struct. 695–696, 39–57.

Bertie, J.E., Morrison, M.M., 1980. The infrared spectra of the hydrates of ammonia, $NH_3{\cdot}H_2O$ and $2NH_3{\cdot}H_2O$ at 95 K. J. Chem. Phys. 73, 4832–4837.

Bézard, B., Drossart, P., Encrenaz, T., Feuchtgruber, H., 2001. Benzene on the giant planets. Icarus 154, 492–500.

Bohn, R.B., Sandford, S.A., Allamandola, L.J., Cruikshank, D.P., 1994. Infrared spectroscopy of Triton and Pluto ice analogs: The case for saturated hydrocarbons. Icarus 111, 151–173.

Bohren, C.F., Huffman, D.R., 1983. Absorption and Scattering of Light by Small Particles. Wiley, New York.

Brooke, T.Y., Knacke, R.F., Encrenaz, T., Dossart, P., Crisp, D., Feuchtgruber, H., 1998. Models of the ISO 3-μm reflection spectrum of Jupiter. Icarus 136, 1–13.

Carlson, B.E., Prather, M.J., Rossow, W.B., 1987. Cloud chemistry on Jupiter. Astrophys. J. 322, 559–572.

Carlson, B.E., Rossow, W.B., Orton, G.S., 1988. Cloud microphysics of the giant planets. J. Atmos. Sci. 45, 2066–2081.

Clapp, M.L., Miller, R.E., 1993. Shape effects in the infrared spectrum of ammonia aerosols. Icarus 105, 529–536.

Dawes, A., Mukerji, R.J., Davis, M.P., Holtom, P.D., Hoffmann, S.V., Shaw, D.A., Mason, M.J., 2007. Morphological study into the temperature dependence of solid ammonia under astrochemical conditions using vacuum ultraviolet and Fourier-transform infrared spectroscopy. J. Chem. Phys. 126, 244711.

de Pater, I., Dunn, D., Romani, P., Zahnle, K., 2001. Reconciling Galileo Probe data and ground-based radio observations of ammonia on Jupiter. Icarus 149, 66–78.

Ferraro, J.R., Sill, G., Fink, U., 1980. Infrared intensity measurements of cryodeposited thin films of NH_3, NH_4HS, H_2S, and assignments of absorption bands. Appl. Spectrosc. 34, 525–533.

Fink, U., Sill, G.T., 1982. The infrared spectral properties of frozen volatiles. In: Wilkening, L. (Ed.), Comets. Univ. of Arizona Press, Tucson, AZ, pp. 164–202.

Friedson, A.J., Orton, G.S., 1999. A dynamical model of Jupiter's 5-micron hot spots. Bull. Am. Astron. Soc. 31, 1155.

Friedson, A.J., Wong, A.S., Yung, Y.L., 2002. Models for polar haze formation in Jupiter's stratosphere. Icarus 158, 389–400.

Gerakines, P.A., Schutte, W.A., Ehrenfreund, P., 1996. Ultraviolet processing of interstellar ice analogs. I. Pure ices. Astron. Astrophys. 312, 289–305.

Gierasch, P.J., Conrath, B.J., Magalhães, J.A., 1986. Zonal mean properties of Jupiter's upper troposphere from Voyager infrared observations. Icarus 67, 456–483.

Grevesse, N., Asplund, M., Sauval, A.J., 2007. The solar chemical composition. Space Sci. Rev. 130, 105–114.

Heavens, O.S., 1965. Optical Properties of Thin Solid Films. Dover, New York.

Holt, J.S., Sadoskas, D., Pursell, C.J., 2004. Infrared spectroscopy of the solid phases of ammonia. J. Chem. Phys. 120, 7153–7157.

Horn, A.B., Banham, S.F., McCoustra, M.R.S., 1995. Optical effects in the IR reflection-absorption spectra of thin water-ice films on metal substrates. J. Chem. Soc. Faraday Trans. 91, 4005–4008.

Howett, C.J.A., Carlson, R.W., Irwin, P.G.J., Calcutt, S.B., 2007. Optical constants of ammonium hydrosulfide ice and ammonia ice. J. Opt. Soc. Am. B 24, 126–136.

Huffman, D.R., 1975. Optical properties of particulates. Astrophys. Space Sci. 34, 175–184.

Irwin, P.G.J., 1999. Cloud structure and composition of Jupiter's atmosphere. Surveys Geophys. 20, 505–535.

Irwin, P.G.J., Weir, A.L., Taylor, F.W., Calcutt, S.B., Carlson, R.W., 2001. The origin of belt/zone contrasts in the atmosphere of Jupiter and their correlation with 5-μm opacity. Icarus 149, 397–415.

Irwin, P.G.J., Sihra, K., Bowles, N., Taylor, F.W., Calcutt, S.B., 2005. Methane absorption in the atmosphere of Jupiter from 1800 and 9500 cm^{-1} and implications for vertical cloud structure. Icarus 176, 255–271.

Irwin, P.G.J., Sromovsky, L.A., Strong, E.K., Sihra, K., Teanby, N.A., Bowles, N., Calcutt, S.B., Remedios, J.J., 2006. Improved near-infrared methane band models and k-distribution parameters from 2000 to 9500 cm^{-1} and implications for interpretation of outer planet spectra. Icarus 181, 309–319.

Khare, B.N., Sagan, C., Arakawa, E.T., Suits, F., Callcott, T.A., Williams, M.W., 1984. Optical constants of organic tholins produced in a simulated titanian atmosphere: From soft X-ray to microwave frequencies. Icarus 60, 127–137.

Kim, S.J., Caldwell, J., Rivolo, A.R., Wagener, R., Orton, G.S., 1985. Infrared polar brightening on Jupiter. III. Spectrometry from the Voyager 1 IRIS Experiment. Icarus 64, 233–248.

Lewis, J.S., 1969. The clouds of Jupiter and the NH_3–H_2O and NH_3–H_2S systems. Icarus 10, 365–378.

Lynch, D.W., Hunter, W.R., 1985. Optical constants of metals. In: Palik, E.D. (Ed.), Handbook of Optical Constants of Solids. Academic Press, New York, pp. 275–359.

Martonchik, J.V., Orton, G.S., Appleby, J.F., 1984. Optical properties of NH_3 ice from the far infrared to the near ultraviolet. Appl. Opt. 23, 541–547.

Matcheva, K.I., Conrath, B.J., Gierasch, P.J., Flasar, F.M., 2005. The cloud structure of the jovian atmosphere as seen by the Cassini/CIRS experiment. Icarus 179, 432–448.

Mishchenko, M.I., Travis, L.D., 1998. Capabilities and limitations of a current FORTRAN implementation of the T-matrix method for randomly oriented, rotationally symmetric scatterers. J. Quant. Spectrosc. Radiat. Trans. 60, 309–324.

Mishchenko, M.I., Travis, L.D., Lacis, A.A., 2005. Scattering, absorption, and emission of light by small particles, second electronic edition. NASA Goddard Institute for Space Studies (available at http://www.giss.nasa.gov/~crmim/books.html).

Moore, M.H., Hudson, R.L., 2003. Infrared study of ion-irradiated N_2-dominated ices relevant to Triton and Pluto: Formation of HCN and HNC. Icarus 161, 486–500.

Moore, M.H., Ferrante, R.F., Hudson, R.L., Stone, J.N., 2007. Ammonia-water ice laboratory studies relevant to outer Solar System surfaces. Icarus 190, 260–273.

Moreno, F., 1996. The structure of the stratospheric aerosol layer in the equatorial and south polar regions of Jupiter. Icarus 124, 632–644.

Ordal, M.A., Long, L.L., Bell, R.J., Bell, E.E., Bell, R.R., Alexander, J.R.W., Ward, C.A., 1983. Optical properties of the metals Al, Co, Cu, Au, Fe, Pb, Ni, Pd, Pt, Ag, Ti, and W in the infrared and far infrared. Appl. Opt. 22, 1099–1119.

Pollack, J.B., Rages, K., Pope, S.K., Tomasko, M.G., Romani, P.N., Atreya, S.K., 1987. Nature of the stratospheric haze on Uranus—Evidence for condensed hydrocarbons. J. Geophys. Res. 92, 15037–15065.

Pryor, W.R., Hord, C.W., 1991. A study of photopolarimeter system UV absorption data on Jupiter, Saturn, Uranus, and Neptune: Implications for auroral haze formation. Icarus 91, 161–172.

Rages, K., Beebe, R., Senske, D., 1999. Jovian stratospheric hazes: The high phase angle view from Galileo. Icarus 139, 211–226.

Reuter, D.C., Simon-Miller, A.A., Lunsford, A., Baines, K.H., Cheng, A.F., Jennings, D.E., Olkin, C.B., Spencer, J.R., Stern, S.A., Weaver, H.A., Young, L.A., 2007. Jupiter cloud composition, stratification, convection, and wave motion: A view from new horizons. Science 318, 223–225.

Robertson, C.W., Downing, H.D., Curnutte, B., Williams, D., 1975. Optical constants of solid ammonia in the infrared. J. Opt. Soc. Am. 65, 432–435.

Rossow, W.B., 1978. Cloud microphysics—Analysis of the clouds of Earth, Venus, Mars, and Jupiter. Icarus 36, 1–50.

Roux, J.A., Wood, B.E., Smith, A.M., 1979. IR optical properties of thin H_2O, NH_3, and CO_2 cryofilms; AEDC-TR-79-57.

Sill, G., Fink, U., Ferraro, J.R., 1981. The infrared spectrum of ammonia hydrate: Explanation for a reported ammonia phase. J. Chem. Phys. 74, 997–1000.

Simon-Miller, A.A., Banfield, D., Gierasch, P.J., 2001. Color and the vertical structure in Jupiter's belts, zones, and weather systems. Icarus 154, 459–474.

Smith, P.H., Tomasko, M.G., 1984. Photometry and polarimetry of Jupiter at large phase angles. II. Polarimetry of the south tropical zone, south equatorial belt, and the polar regions from the Pioneer 10 and 11 missions. Icarus 58, 35–73.

Strobel, D.F., 1973. The photochemistry of NH_3 in the jovian atmosphere. J. Atmos. Sci. 30, 1205–1209.

Szymanski, H.A., 1964. Interpreted Infrared Spectra, vol. 1. Plenum, New York.

Teolis, B.D., Loeffler, M.J., Raut, U., Famá, M., Baragiola, R.A., 2007. Infrared reflectance spectroscopy on thin films: Interference effects. Icarus 190, 274–279.

Tomasko, M.G., Karkoschka, E., Martinek, S., 1986. Observations of the limb darkening of Jupiter at ultraviolet wavelengths and constraints on the properties and distribution of stratospheric aerosols. Icarus 65, 218–243.

Tomasko, M.G., West, R.A., Orton, G.S., Tejfel, V.G., 1984. Clouds and aerosols in Saturn's atmosphere. In: Gehrels, T., Matthews, M.S. (Eds.), Saturn. Univ. of Arizona Press, Tucson, pp. 150–194.

Tompkins, H.G., McGahan, W.A., 1999. Spectroscopic Ellipsometry and Reflectrometry: A User's Guide. Wiley, New York.

Weidenschilling, S.J., Lewis, J.S., 1973. Atmospheric and cloud structures of the jovian planets. Icarus 20, 465–476.

West, R.A., Orton, G.S., Draine, B.T., Hubbell, E.A., 1989. Infrared absorption features for tetrahedral ammonia ice crystals. Icarus 80, 220–223.

West, R.A., Baines, K.H., Friedson, A.J., Banfield, D., Ragent, B., Taylor, F.W., 2004. Jovian clouds and haze. In: Bagenal, F., Dowling, T.E., McKinnon, W.B. (Eds.), Jupiter. Cambridge Univ. Press, Cambridge, pp. 79–104.

Wong, A.S., Lee, A.T.T., Yung, Y.L., Ajello, J.M., 2000. Jupiter: Aerosol chemistry in the polar atmosphere. Astrophys. J. 534, L215–L217.

Wong, A.S., Yung, Y.L., Friedson, A.J., 2003. Benzene and haze formation in the polar atmosphere of Jupiter. Geophys. Res. Lett. 30, 1–4.

Wong, M.H., Bjoraker, G.L., Smith, M.D., Flasar, F.M., Nixon, C.A., 2004. Identification of the 10-μm ammonia ice feature on Jupiter. Planet. Space Sci. 52, 385–395.

Wong, M.H., Lunine, J., Atreya, S.K., Johnson, T., Mahaffy, P.R., Owen, T.C., Encrenaz, T., 2008. Oxygen and other volatiles in the giant planets and their satellites. In: MacPherson, G.J., Mittlefehldt, D.W., Jones, J., Simon, S.B., Mackwell, S. (Eds.), Oxygen in the Earliest Solar System. In: Reviews in Mineralogy and Geochemistry, vol. 68. Mineralogical Society of America, Chantilly, VA, pp. 219–246.

Yeh, P., 1998. Optical Waves in Layered Media. Wiley, Hoboken.